JOURNAL OF GEOPHYSICAL RESEARCH, VOL. 115, A03203, doi:10.1029/2009JA014415, 2010

Three-dimensional hybrid simulation of magnetosheath reconnection under northward and southward interplanetary magnetic field

Y. Pang,[1,2] Y. Lin,[2] X. H. Deng,[1] X. Y. Wang,[2] and B. Tan[2]

Received 30 April 2009; revised 21 September 2009; accepted 5 October 2009; published 5 March 2010.

[1] A three-dimensional (3-D) global hybrid simulation is carried out for the generation and structure of magnetic reconnection in the magnetosheath because of the interaction of an interplanetary tangential discontinuity (TD) with the bow shock and magnetosphere. Runs are performed for solar wind TDs possessing different polarization senses of magnetic field (north-to-south or south-to-north from the leading to trailing side of the incident TD) and initial half-widths. Two-step compression processes are shown in the transmitted TD, including a "shock compression," as the TD passes through the shock followed by a subsequent "convective compression" while the TD is moving in the magnetosheath toward the magnetopause. In cases with a relatively thin solar wind TD, 3-D patchy reconnection is initiated in the transmitted TD, forming magnetosheath flux ropes. Differences between these flux ropes and those due to magnetopause reconnection are discussed. Multiple components of ion particles are present in the velocity distribution in the magnetosheath merging, accompanied by ion heating. For cases with a relatively wide initial TD, a dominant single *X* line appears in the subsolar magnetosheath after the transmitted TD is narrowed through the two-step compression process. Specifically, in the cases with a south-to-north field rotation across an incident thin TD, the magnetosheath flux ropes could re-reconnect with the closed geomagnetic field lines to generate a closed field line region with mixed magnetosheath and magnetospheric plasmas, which may contribute to the transport of solar wind plasma into the magnetospheric boundary layer.

Citation: Pang, Y., Y. Lin, X. H. Deng, X. Y. Wang, and B. Tan (2010), Three-dimensional hybrid simulation of magnetosheath reconnection under northward and southward interplanetary magnetic field, *J. Geophys. Res.*, *115*, A03203, doi:10.1029/2009JA014415.

1. Introduction

[2] Solar wind directional discontinuities are abrupt rotations of the heliospheric magnetic field across layers that are observed approximately every 30 min near 1 AU [*Burlaga et al.*, 1977] and thus are a common phenomenon in space. Primarily, two types of directional discontinuities are often present in the solar wind: (1) rotational discontinuities, or large-amplitude Alfvén waves, which possess a finite normal component of the magnetic field, and (2) tangential discontinuities, which are static magnetic boundaries or current sheets without a normal field component. These discontinuities are considered to be associated with many physical processes occurring in the Earth's magnetosphere and ionosphere. They are believed to cause rapid equatorward movement of aurora and sudden changes of the *H*-component geomagnetic field at high-latitude geomagnetic stations [*Øieroset et al.*, 1996]. Northward turning of the interplanetary magnetic field (IMF), which could also be viewed as a solar wind discontinuity, has often been referred to as a trigger of the substorm expansion onset [*Lyons et al.*, 1997]. The formation of a strong geomagnetic storm is found to be favored by an extended period of southward IMF that is preceded by an earlier interval of northward field or very weak B_Z [*Thomsen et al.*, 2003].

[3] Magnetic reconnection [*Dungey*, 1961] is believed to be a fundamental plasma process in a current sheet, which converts the magnetic energy into particle energy, leading to heating and abrupt acceleration of both ions and electrons [*Krauss-Varban and Omidi*, 1995; *Lin and Swift*, 1996; *Fu et al.*, 2006; *Pritchett*, 2006]. Numerous burst events in space plasmas have been confirmed by in situ observations to be associated with magnetic reconnection. Reconnection at the Earth's magnetopause [*Sonnerup et al.*, 1995] provides an efficient mechanism for transfer of solar wind mass, momentum, and energy into the magnetosphere. Evidence of near-Earth and distant magnetotail reconnection has also been reported [e.g., *Øieroset et al.*, 2001; *Borg et al.*, 2005]. In the solar wind, some reconnection exhausts have been discovered [*Gosling et al.*, 2005], with a large-scale reconnection *X* line extending at least hundreds of Earth radii

[1]Department of Space Physics, Wuhan University, Wuhan, China.
[2]Physics Department, Auburn University, Auburn, Alabama, USA.

0148-0227/10/2009JA014415$09.00

[*Phan et al.*, 2006]. In situ observations have also provided evidence of reconnection in a turbulent plasma downstream of the bow shock [*Retin et al.*, 2007]. All these observations suggest that magnetic reconnection is a universal process and plays an important role in physical processes in the coupled Sun-Earth plasma system.

[4] Magnetohydrodynamic (MHD) simulation using the Integrated Space Weather Prediction Model (ISM) has predicted the merging of interplanetary magnetic field lines in the magnetosheath across opposite sides of a directional discontinuity from the solar wind [*Maynard et al.*, 2002]. The result of a two-dimensional (2-D) hybrid simulation [*Lin*, 1997] has also suggested the magnetosheath reconnection as a consequence of the compression of a solar wind current sheet at the bow shock. Such a prediction has recently been confirmed by observations of Cluster spacecraft [*Phan et al.*, 2007]. When Cluster 1 was located at a magnetosheath location of [6.7, 2.0, −9.5] R_E in the GSE coordinate system, a current sheet with a width of 525 km or 10 local ion skin depths was found to be accompanied by enhanced flow, density, and ion temperature. Correspondingly, a rather wide current sheet (about 3 R_E or 264 local ion skin depths) was also observed in the solar wind by ACE satellite, and an examination indicated that the thinner one was due to the wider sheet being compressed when propagating into the magnetosheath. How such a wide current sheet is narrowed so significantly to initiate the reconnection when it interacts with the bow shock and magnetopause remains an important issue of study.

[5] In *Phan et al.*'s [2007] case, the magnetic field changes orientation from the north to south across the solar wind directional discontinuity. No dayside magnetopause reconnection is expected under the northward IMF before the current sheet arrives. Such a case under an initially northward IMF was recently investigated by *Omidi et al.* [2009] through a 2-D hybrid simulation study of magnetosheath reconnection caused by the interaction among TD, bow shock, and magnetopause. Both quasi-steady reconnection and time-independent reconnection were obtained because of different initial widths of TD.

[6] A related question to ask is: What if the solar wind condition is different so that the IMF changes direction from the south to north? In this situation, reconnection could also occur between field lines of the IMF and magnetosphere, on the earthward side of the transmitted TD. The two simultaneous reconnection events at the magnetopause and in the magnetosheath could compete with each other to consume the magnetic field energy sandwiched by them, which may affect the magnetosheath reconnection. Meanwhile, the paraboloidal-like configuration of the bow shock and magnetopause on the dayside is expected to introduce 3-D features to the reconnection process.

[7] In this paper, we present a 3-D global hybrid simulation of the interaction between an interplanetary directional TD and the dayside bow shock and magnetopause. Hybrid simulations have been used to address the large-scale structure and associated ion dynamics in magnetic reconnection [e.g., *Krauss-Varban and Omidi*, 1995; *Lin and Swift*, 1996; *Lottermoser et al.*, 1998; *Lin*, 2001; *Omidi and Sibeck*, 2007]. The focus of the present investigation is on the magnetic field structure and ion particle signatures associated with the magnetosheath reconnection, under different conditions of the IMF direction change across the solar wind TD. Differences between the magnetosheath merging processes corresponding to the north-to-south and south-to-north field rotations are addressed. The evolution of the transmitted TD with different initial widths of TD is also studied. Hereinafter, we will use the terms "merging layer" and "reconnection current sheet" for the current layer in which the magnetosheath reconnection has been initiated and "transmitted TD" and "transmitted current sheet or layer" to describe the transmitted part of the initial tangential discontinuity in general.

[8] The outline of the paper is as follows. The simulation model is described in section 2. In section 3, we present the simulation results for four cases with different IMF rotation senses and initial half-width of the solar wind TD. Discussions of the simulation results and the conclusion are given in section 4.

2. Simulation Model

[9] The 3-D global hybrid code utilized here is similar to that used by *Lin and Wang* [2005] for the dayside bow shock–magnetosphere system. The detailed code description can be found by *Swift* [1996]. In the hybrid model, ions (protons) are treated as fully kinetic particles and electrons are treated as a massless fluid. The simulation domain contains the dayside plasma regions, with GSE $X > 0$, within the geocentric distance $4R_E < r < 25R_E$. A spherical coordinate system is applied in the calculation, in which the polar axis is chosen as the GSE Y axis. The polar boundaries of the domain are set at the 20° and 160° polar angles to avoid singular coordinate lines along the Y axis. The dayside geomagnetic polar regions, around the Z axis, are kept in the domain.

[10] The initial condition includes a dipole geomagnetic field plus a mirror dipole in $r < 10R_E$ and a uniform solar wind in $r > 10R_E$, in which the initial IMF can be assumed in an arbitrary direction. The mirror dipole is used in the initial setup to speed up the evolution process of the solar wind–magnetosphere interaction without losing the key physical features. The bow shock, magnetosheath, and magnetopause are formed by the interaction between the solar wind and the dipole field.

[11] For cases shown in this paper, in which the initial IMF is either purely northward or purely southward, the propagation direction of interplanetary TD is along the $-X$ direction as the TD convects earthward with the solar wind. Initially at $t = 0$, the interplanetary TD is assumed to be located at a distance corresponding to $X = 30R_E$ outside the simulation domain. Along the frontside boundary at $X = 25R_E$, the magnetic field across the TD is described by

$$B_x = 0, \quad B_y = -B_0 \sin(\phi(X)), \quad B_z = B_0 \cos[\phi(X)], \tag{1}$$

$$\varphi(X) = \Delta\Phi\left(1 + \tanh\left(\frac{X - X_{\mathrm{TD}}(t)}{w}\right)\right)\Big/2, \tag{2}$$

where B_0 is the strength of the unperturbed IMF, $X_{\mathrm{TD}}(t) = 30R_E - V_0 t$ is the X position of the TD center as a function of time, V_0 is the solar wind flow speed, and w is the initial half-width of the TD. The rotation angle of the tangential

Table 1. Initial IMF in the Domain and Magnetic Field Angle Change $\Delta\Phi$ and Half-Width w of the Initial TD, With $\Delta\Phi > 0$ Corresponding to a Southward Change[a]

	Initial IMF	$\Delta\Phi$ (deg)	w
Run 1	northward	180	1 R_E
Run 2	northward	180	3 R_E
Run 3	southward	−180	1 R_E
Run 4	southward	−180	3 R_E

[a]IMF, interplanetary magnetic field.

magnetic field $\Delta\Phi$ is assumed to be positive if the IMF turns from north to south across the TD. The spatial profile described by equations (1) and (2) corresponds to a circularly polarized magnetic field through the initial TD.

[12] A current-dependent anomalous collision frequency $\nu = aJ$ is applied everywhere, where J is the current density and the coefficient a is chosen so that the typical peak collision frequency $\nu \sim 0.01$–$0.1\Omega_0$. The simulation results are found to be insensitive to the magnitude of ν.

[13] In the solar wind, the ion gyrofrequency Ω_0 is chosen to be $1.0s^{-1}$, corresponding to an IMF of ~10 nT and a field of ~50 nT at the subsolar magnetopause. The ion inertial length $d_0 = c/\omega_{p0}$ is chosen to be $0.1R_E$ and the corresponding Alfvén speed $V_{A0} = 0.1R_E/s$. The solar wind speed is assumed to be $V_0 = 5V_{A0}$, corresponding to a Mach number $M_A = 5$. The interplanetary TD enters the simulation domain at $t = 10\Omega_0^{-1}$. Note that the Alfvén speed and thus the solar wind flow speed in the simulation are about 6 times larger than those in reality. Effects of this overlarge Alfvén speed will be discussed later. The solar wind ion plasma beta β_i is set to be 0.5. About 150–400 particles are used in each grid cell for the interested regions of the solar wind, magnetosheath, and magnetopause.

[14] Physical quantities are normalized as follows. The magnetic field B is normalized to the IMF B_0, the ion number density to the solar wind density N_{i0}, the time t to Ω_0^{-1}, and the flow velocities are normalized to V_{A0}. The spatial coordinates are expressed in units of R_E. The thermal pressure is expressed in units of the magnetic pressure $P_{00} = B_0^2/2\mu_0$ and the temperature is in units of P_{00}/N_{i0}.

[15] Four cases are presented in the following. Some parameters of the initial TD in these runs are listed in Table 1. Note that since we use the hyperbolic tangent function to connect the upstream and downstream values of the initial TD, the total width of the initial current sheet, which has been used by *Phan et al.* [2007] to describe the observed TD, is roughly 3 times the half-width.

3. Simulation Results

3.1. Cases With North-to-South Field Direction Change Across TD

[16] Run 1 corresponds to a case in which a purely northward IMF on the earthward side of an incoming solar wind TD changes direction to point southward behind the discontinuity, with field direction changing by angle $\Delta\Phi = 180°$. The half-width of the initial TD is $w = 1R_E$ or $10d_0$. In this case, the bow shock front is well developed by $t = 30$, while the solar wind TD reaches the shock around $t = 35$. No reconnection occurs in the TD before it reaches the bow shock.

[17] When the planar TD approaches the bow shock and subsequently the magnetopause, it is distorted because of the different degrees of slowing down of the shocked solar wind at different longitudes and latitudes. Meanwhile, the unshocked part of TD is dragged tailward by the solar wind with the unperturbed solar wind velocity. The planar TD thus becomes a paraboloidal structure. Apparently, such a transition from a 1-D to 3-D structure will affect the magnetosheath merging process as the solar wind TD is transmitted into the magnetosheath.

[18] In run 1, after the subsolar part of TD completely passes across the bow shock by $t = 40$, the average central width of transmitted TD has been narrowed down to $0.8R_E$ (nearly one third of the total width just before the TD crosses the bow shock) because of the compression at the shock, a "first step compression." Meanwhile, the magnetic field strength on both sides of the transmitted TD is increased by approximately 3 times. The maximum current density is therefore increased by 9–10 times in our simulation. Magnetosheath reconnection is seen to be initiated in the transmitted TD around $t = 45$. The occurrence of reconnection can be identified by the magnetic field configuration and characteristics of particle acceleration and heating processes (Figures 4 and 5).

[19] Figure 1a shows the magnetic field line geometry in the magnetosheath reconnection and ion density contours in the noon meridian plane obtained from run 1 at $t = 60$. Several 3-D isosurfaces of the magnetic field strength with $B = 1.7$ (colored by blue) are superposed in the plot, indicating regions with a relatively weak field. The ion density structure in the noon meridian plane is also plotted in Figure 1a. The bow shock (magnetopause) is well defined by the sudden increase (decrease) of ion density along the earthward direction.

[20] At $t = 60$, the average width of the transmitted TD has been further reduced because of a "second step compression." Different from the first step shock compression, the second step compression is a subsequent compression when the transmitted TD is moving against the magnetopause. In cases such as run 1 with a relatively thin initial TD, these two compression processes are well separated in time. For a wider TD, however, these two processes may be mixed. The difference between these two steps of compression is discussed later.

[21] The magnetosheath reconnection in run 1 appears to be of a patchy type [*Lee*, 1995], in which the size of each reconnection region has a fairly limited extent and thus the reconnection is a localized and non-steady 3-D structure [*Linton and Longcope*, 2006]. The three bundles of field lines (yellow, green, and red) shown in Figure 1a are open field lines with both ends connected to the IMF. The red ones and yellow ones are the field lines that are reconnected only once, while the green field lines are the ones reconnected more than once. The difference between these two types of field lines can be seen in the zoomed-in pictures in Figures 1c and 1d, for areas centered at the magenta dots. As shown in Figure 1c, the flux tubes represented by the red field lines and those by the yellow ones can travel in an unconstrained manner in the corresponding directions or, in other words, they are unconnected with each other, as expected for a patchy reconnection [*Otto*, 1995]. Note that the average field strength in the magnetosheath is about 3–4.

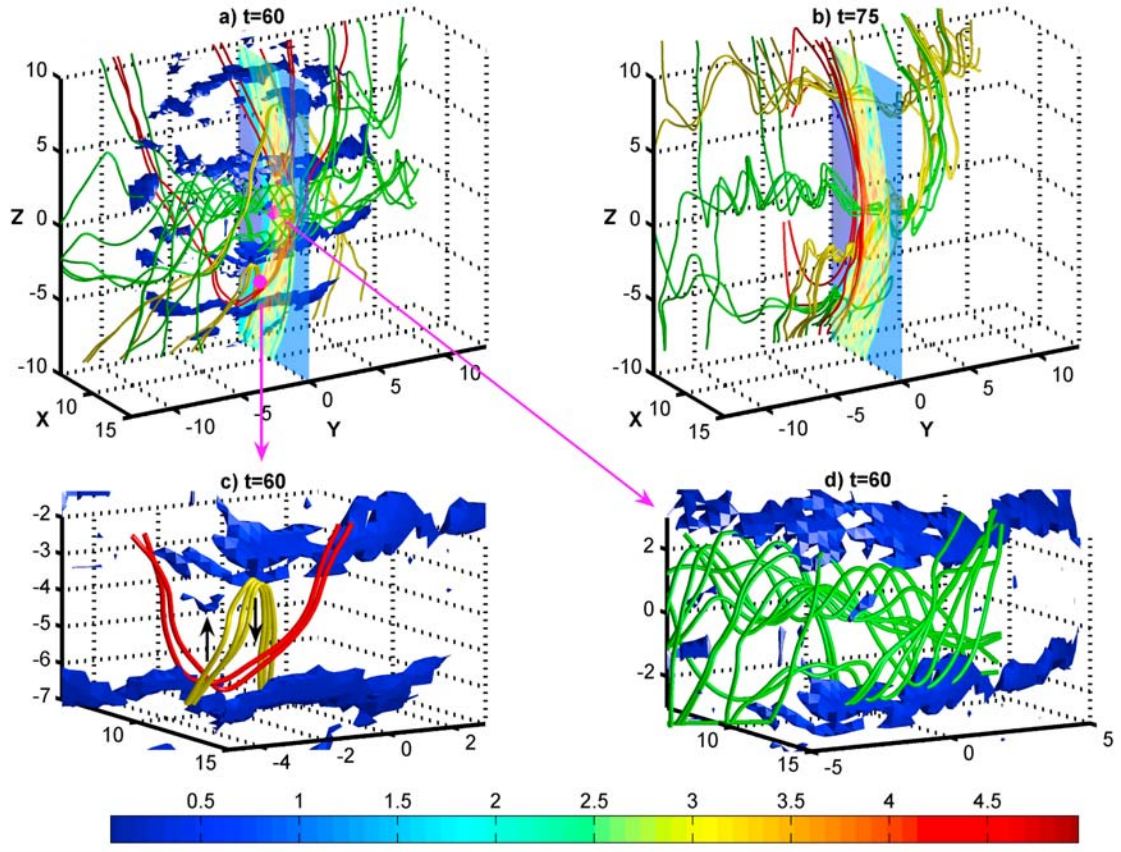

Figure 1. (a) Magnetosheath patchy reconnection in run 1 at $t = 60$. The color-coded contours indicate ion density in the $Y = 0$ plane. Three bundles of open field lines are colored by yellow, green, and red. Blue isosurfaces represent a weak magnetic field region inside the merging layers, where $B = 1.7$. (b) Magnetosheath flux ropes in run 1 at $t = 75$. Red field lines are some closed and open lines on the earthward side of the magnetosheath merging layer. Yellow and green field lines are the magnetosheath flux ropes produced by the patchy reconnection. Characteristic field lines from (c) region $6R_E < x < 15R_E$, $-5R_E < y < 3R_E$, $-7R_E < z < -2R_E$ and (d) region $6R_E < x < 15R_E$, $-5R_E < y < 5R_E$, $-3R_E < z < 3R_E$ show two types of field lines during the evolution of patchy reconnection.

There are mainly four stripe-like low field regions at $t = 60$, as shown by the isosurfaces in Figure 1a, which are centered around $Z = -7$, -2.4, 2.4, and $7.8R_E$. The regions could not be considered as single X lines, but should be viewed as time-dependent reconnection events with groups of localized multiple X lines. These "reconnection pools" can extend over the entire dayside magnetosheath in the dawn-dusk direction. No apparent steady single X line is found in this case.

[22] A direct consequence of these patchy reconnection events is the distorted spiral magnetic field lines, i.e., the magnetosheath flux ropes, as indicated by the green field lines in Figures 1a and 1d. Magnetic flux tubes are narrowed, and the magnetosheath plasma is "squeezed" because of the high-speed flows directed in opposite directions (indicated by the black arrows in Figure 1c) generated by the reconnection processes that take place in the neighboring reconnection pools or patches, which carry both flux tubes and plasmas in opposite directions and produce flux ropes as predicted by the patchy reconnection model. Enhancement of the Y-component magnetic field and the density can be found at the center of the magnetosheath flux ropes. Such patchy structure indicates a mechanism of reconnection very different from the 2-D process.

[23] Figure 1b displays the later stage of these patchy reconnection structures at $t = 75$. For comparison, some magnetic field lines (red), including both the closed and open ones, on the earthward side of the transmitted current layer are also shown in Figure 1b. At this time, the flux tubes are more distorted, and their north–south scale lengths are narrowed to about $1.5–2.5R_E$. These reconnection flux tubes carried by the transmitted current layer have reached the magnetopause, piling up with the ambient field lines against the pause. Because of the magnetosheath flow, they convect azimuthally and tailward along the magnetopause, as to be demonstrated in Figures 2 and 3. At $t = 80$, the magnetopause reconnection is initiated, indicating that the magnetic fluxes on the sunward side of the transmitted current layer have reached the magnetopause and begin to interact with the pause.

[24] To illustrate the evolution of the magnetosheath merging layer, we show in Figure 2 the B_y component of the magnetic field in the $Y = 0$ plane at $t = 45$, 60, 70, and 75. Originally in the incident TD upstream of the shock, B_y is

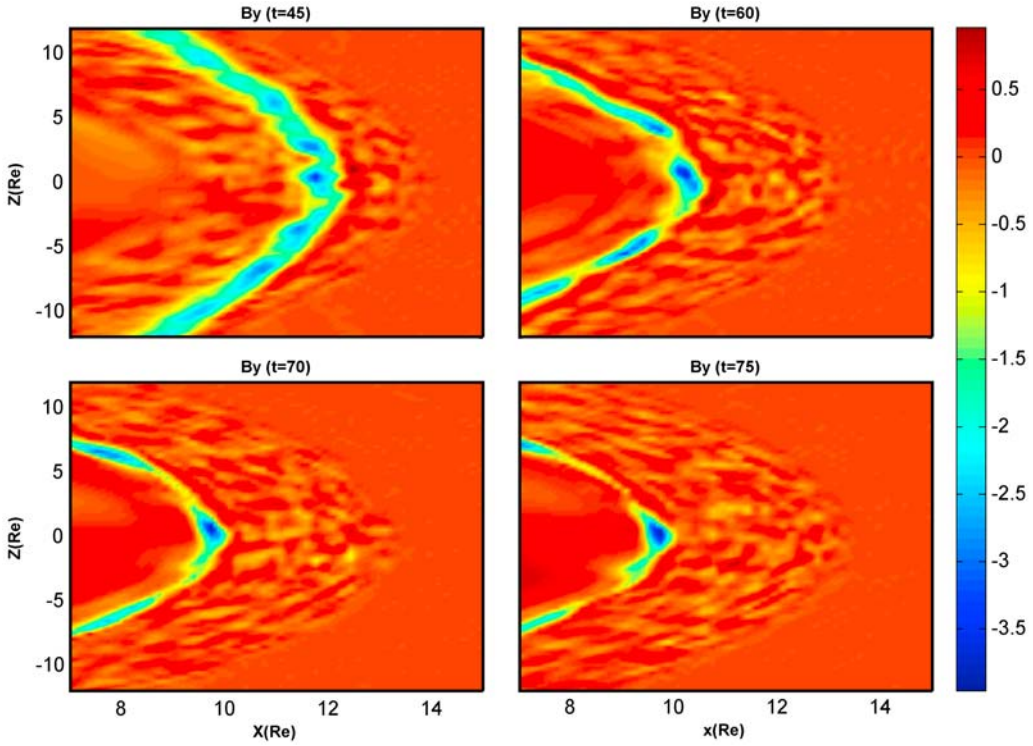

Figure 2. Evolution of B_Y in the $Y = 0$ plane obtained in run 1 at $t = 45$, 60, 70, and 75.

nearly uniform along the Z direction. In the transmitted TD, however, the B_y structure becomes nonuniform with the evolution of merging layers, as seen in Figure 2. Bundles of Y-component fluxes are formed at $t = 60$, 70, and 75. Although reconnection may be initiated at different sites and/or influenced by fluctuations downstream of the bow shock, which will be discussed later, once reconnection takes place in a certain region, the newly generated high-speed flow

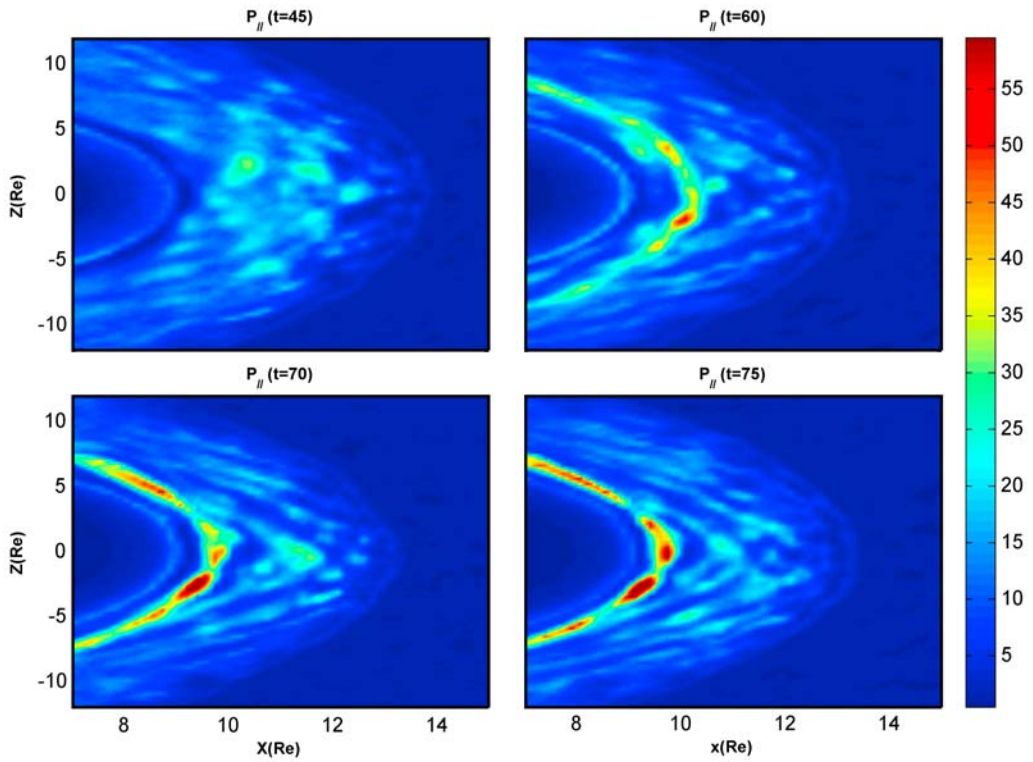

Figure 3. Same as Figure 2, except for parallel pressure.

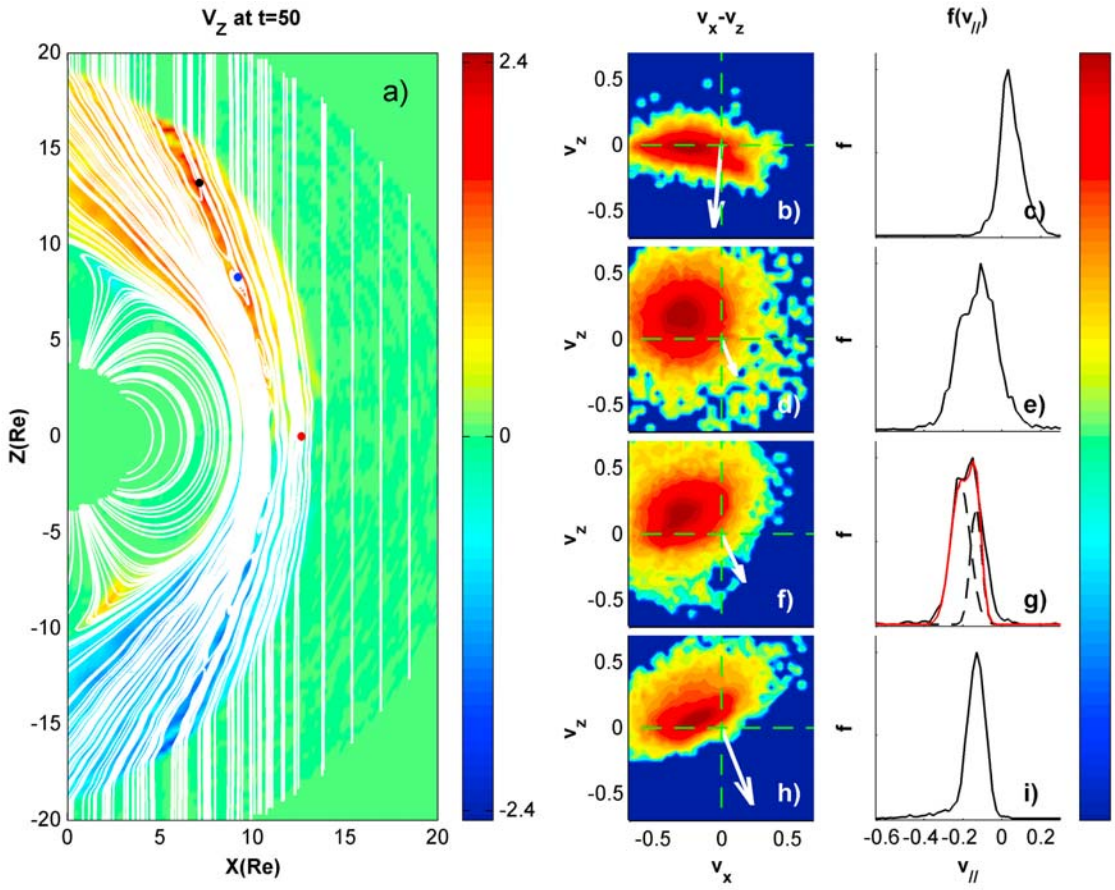

Figure 4. (a) Z-component ion bulk velocity and field line projection in the $Y = 0$ plane in run 1 at $t = 50$. (b–i) Typical ion velocity distributions in the v_x–v_z plane and the line-cut distribution functions $f(v_{\|})$ at $v_{\perp} = V_{\perp}$ along the local magnetic field taken at various locations and times around the magnetosheath reconnection.

sweeps out the Y-component magnetic fluxes, leading to the local reduction of B_y, as seen from Figure 2a. Such reduction causes the decrease in magnetic pressure and makes the region narrower, locally more antiparallel field like, and thus more preferable for reconnection. These two processes (sweeping and reconnection) boost each other to produce bundles of the B_y flux shown in Figures 2b–2d. Thinning of the current sheet would also occur for a TD with a linear magnetic field polarization because of the plasma outflow ejection of reconnection. The bundles of Y-component fluxes that are located at [9.15, 0, −5] at $t = 60$ have moved to [8, 0, −6] at $t = 70$, which gives a convection speed of nearly 0.18, consistent with the magnetosheath flow in the corresponding region. Time evolution of the parallel pressure is shown in Figure 3, with the same format as Figure 2. The high parallel pressure regions shown by the contours are located near and inside the magnetosheath flux ropes (reconnection exhausts) and so are the high parallel temperature regions (not shown). This result is consistent with previous simulations and observations of reconnection [e.g., *Hoshino et al.*, 1998]. The pressure increase is stronger toward later stages of the merging process.

[25] Figure 4a displays contours of the V_z component of ion bulk-flow velocity at $t = 50$ in the $Y = 0$ plane. Magnetic field lines projected to $Y = 0$ are also superposed on the plot, which show multiple locations of reconnection sites in the transmitted current sheet. High-speed flows are present in the reconnected current sheet. The middle part of Figure 4 shows ion velocity distributions in the v_x–v_z space, while the black solid curves in the right part show the corresponding line-cut distribution functions $f(v_{\|})$ at $v_{\perp} = V_{\perp}$ along the local magnetic field, where v represents the ion particle velocity. The white arrows in Figure 4 indicate the projected direction of the magnetic field. Ions in the upstream solar wind can be well described by a cold, drifting Maxwellian distribution with bulk flow centered at $V_X = -0.5$ (not shown). Upon transmitted into the shocked solar wind, these ions are strongly heated in the perpendicular direction. In our case, the subsolar magnetosheath is the downstream region of a near perpendicular shock. An anisotropic pancake-shaped downstream distribution is present, with perpendicular temperature much larger than the parallel temperature [*Lin and Wang*, 2006], as shown in Figure 4b for particles sampled at the red dot in Figure 4a at $t = 50$.

[26] Figures 4d–4i summarize typical velocity distributions in the high-speed flow region of magnetosheath reconnection. Distributions at the blue dot in Figure 4a are shown in Figures 4d and 4e. The contours in Figure 4d clearly reveal a much more isotropic structure than those in Figure 4b at the red dot outside the reconnection region,

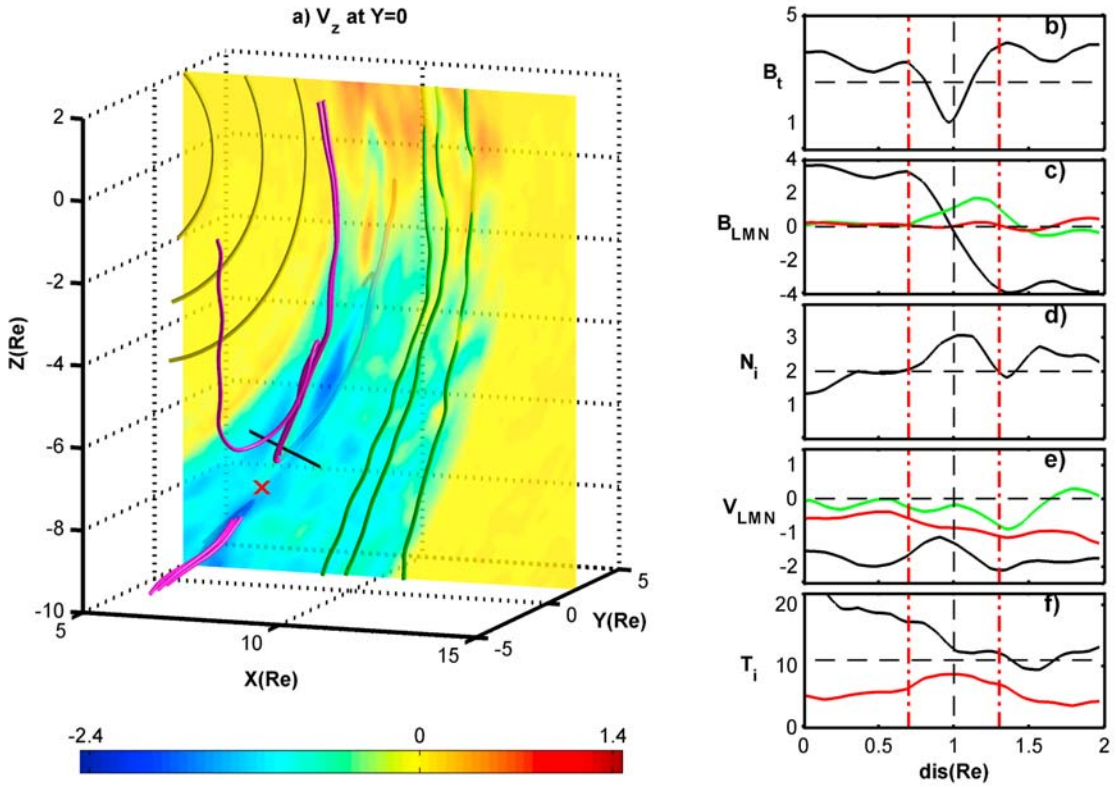

Figure 5. (a) Some reconnected field lines (magenta) around magnetosheath reconnection sites, closed field lines (yellow) inside the magnetosphere, open magnetosheath field lines (green), and contours of ion bulk V_z in the $Y = -2$ plane. Also shown are spatial profiles of (b) magnetic field strength, (c) field components B_L (black), B_M (green), and B_N (red) in the LMN coordinate system, (d) ion number density, (e) ion bulk flow in the LMN coordinates, and (f) ion temperatures $T_{||}$ (red) and $T_{\perp}$ (black) along the black path in Figure 5a, near the reconnection site marked by the cross, as functions of an outbound distance.

while the distribution function $f(v_{||})$ in Figure 4e is found to be composed of two ion populations. Similar distributions are also seen further north around the black dot in Figure 4a, shown in Figures 4f and 4g. This distribution is taken on the sunward side in the transmitted current layer, as evidenced by the southward magnetic field direction indicated by the arrow in Figure 4d. The presence of the two ion populations can be seen from the two dashed lines in Figure 4g, which indicate two Maxwellian fits with different temperatures based on the simulation result. The red solid line indicates the sum of the two dashed populations. Both populations are centered at bulk velocities $V_{||} < 0$, but the hotter population appears to be a direct consequence of the magnetosheath reconnection. The colder, slightly slower population represents the inflow magnetosheath beam in the reconnection current sheet. Note that the observed magnetosheath merging [*Phan et al.*, 2007] also shows that the high-speed flow is accompanied by a strong particle heating. Ion heating as well as acceleration due to reconnection in a nearly symmetric current layer, as in the case of magnetosheath reconnection, has also been reported in earlier simulations [*Krauss-Varban and Omidi*, 1995; *Lin and Swift*, 1996]. Notice the imperfect match between the simulated and the red fitted curve toward the $v_{||} > 0$ side, which may indicate that the divided distributions are not exactly Maxwellian.

[27] Figures 4h and 4i present distributions at, again, the blue dot but at a later time $t = 65$. At this moment, the transmitted current sheet has moved further earthward, leaving the blue location behind the reconnection region. The ion distributions here appear similar to those shown in Figures 4b and 4c for the typical magnetosheath plasma downstream of the quasi-perpendicular shock. In order to compare our simulation with satellite observations of the magnetosheath reconnection [*Phan et al.*, 2007], Figures 5b–5f display the spatial profiles of various quantities along an outbound path through a reconnection current sheet obtained in run 1. The path is drawn with a black line in Figure 5a, which shows some field lines as well as the V_Z contours in the $Y = 2$ plane at $t = 65$. Three bundles of field lines are shown, with yellow ones representing the closed lines in the magnetosphere, green ones for open interplanetary field lines sunward of the merging layer, and magenta ones being the field lines inside the magnetosheath merging layer. At this moment, the merging layer has warped around the magnetopause. An X line is seen around the location of $[7, 2, -8]R_E$, just below the black path, as indicated by the red cross in Figure 5a. The IMF conditions in run 1, with a north-to-south field rotation, are similar to those in the observed event on 14 January 2003, in which Cluster 1 spacecraft also identified reconnection signatures in the southern hemisphere near the path in Figure 5a.

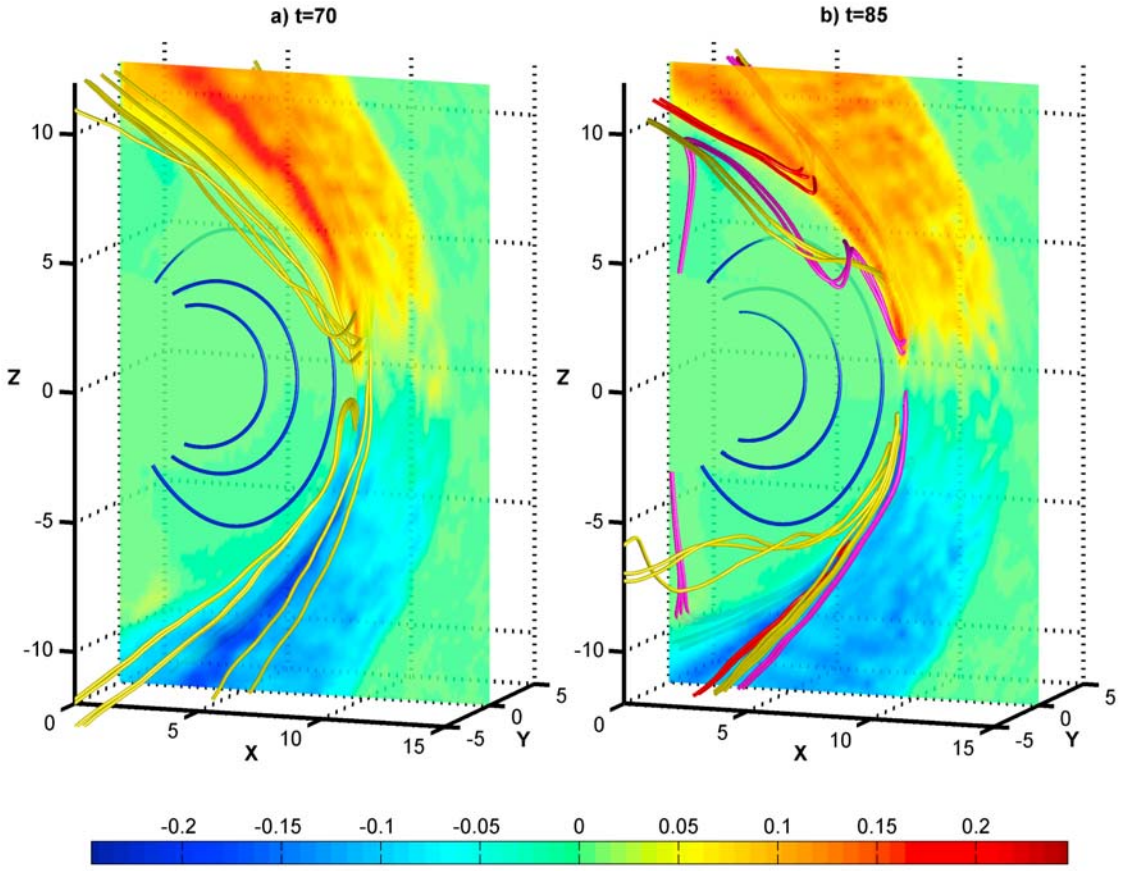

Figure 6. (a) Magnetosheath reconnection in run 2 dominated by a single X line near the subsolar region. (b) At a later time, it coexists with the magnetopause reconnection when the transmitted solar wind current sheet interacts with the magnetopause.

[28] The two vertical dotted-dashed lines in Figures 5b–5f bound the central region of the transmitted TD or the reconnection current sheet. The magnetic field strength along the outbound path shows a dip on the earthward side of the reconnection current sheet, as can be seen in Figure 5b. Figures 5c and 5e show the components of magnetic field and ion bulk velocity, respectively, in the LMN coordinate system [*Russell and Elphic*, 1979], where the orientations of the local normal (N) and tangential (L and M) directions are determined by the Minimum Variance Analysis (MVA) technology [*Sonnerup and Cahill*, 1967]. Component B_N normal to the current sheet remains to be a small constant, while the B_L component, which is mainly along the north–south direction, reverses sign across the current sheet. The guide field component B_M appears to have a stronger positive (dawnward) enhancement on the sunward side than the earthward side, which could be considered as a shifting quadruple B_M structure associated with the Hall effects [*Borg et al.*, 2005]. Note that for initial discontinuity with an imposed finite B_Y, it tends to maintain the net value of the integrated B_M flux through the current sheet because of the conservation of tangential electric field. These features in the magnetic field structure resemble those observed in the magnetosheath reconnection events [*Phan et al.*, 2007].

[29] At this duskside location, both V_N and V_M remain to be a nearly constant negative value in the reconnection current sheet. The negative (southward) tangential flow V_L, however, shows a northward enhancement because of the fact that the path, although below the equator, is on the northward side of the X line. Such flow ejection leads to a change in V_L equal to about one Alfvén speed in the solar wind. The ion density also increases in the reconnection current sheet, as shown in Figure 5d. The enhanced density and parallel ion temperature (Figure 5f) are well correlated with the flow jet in V_L, also consistent with the observation results. Different from our results, however, the V_L component of reconnection flow observed by *Phan et al.* [2007] is so strong that it has reversed direction from the ambient southward magnetosheath flow to reach a positive value. One factor that may limit the strength of the reconnection jet in our simulation is the existence of another reconnection X line northward of this X line, near $Z = -2$, as seen in Figure 5a. Another factor that could contribute to this difference may be the lack of a tilt angle of the geomagnetic dipole field in our model. In the satellite observation around UT 0600, the local magnetic latitude is shifted toward the equatorial plane because of the dipole tilt angle, which leads to a smaller southward magnetosheath flow near the satellite path.

[30] With a thicker initial width, the evolution of the current sheet is found to be different from that for a relatively thin sheet in run 1. Figure 6 shows the results of run 2, which are similar to those of run 1 except that a larger half-width of $w = 3R_E$ is assumed in the solar wind TD. The

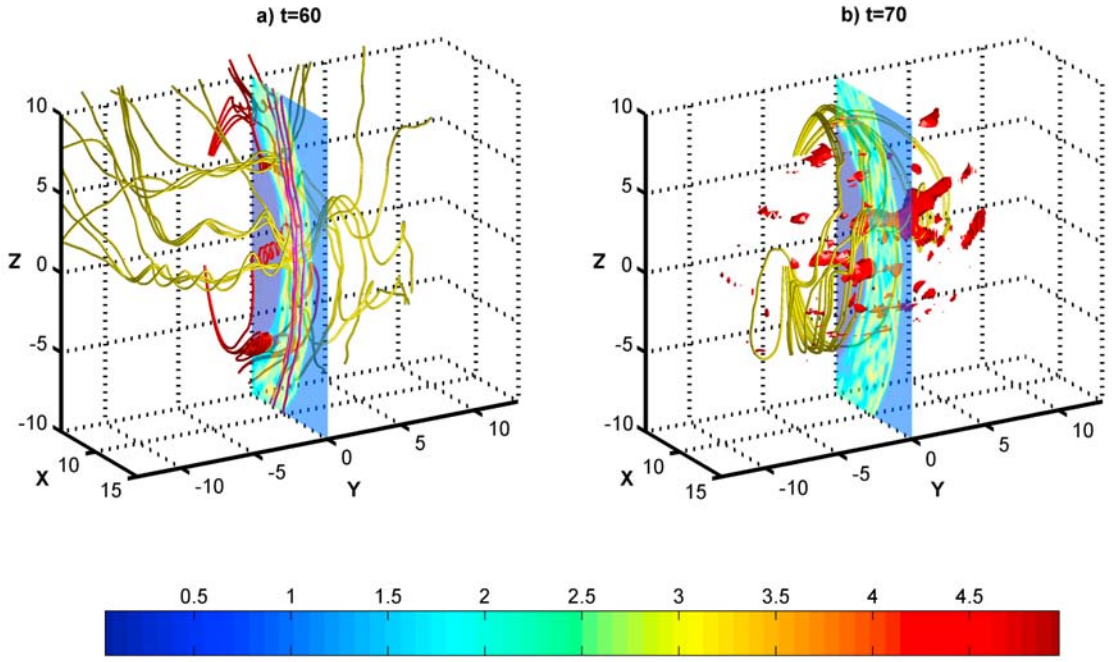

Figure 7. (a) Magnetic field structure in run 3 at t = 60: Magnetosheath flux ropes (yellow) and magnetopause flux ropes (red). (b) Results at t = 70. Red isosurfaces are high-density regions, where the magnetosheath plasma has been captured by newly formed, distorted closed field lines produced by re-reconnection between the geomagnetic field lines and the magnetosheath flux ropes.

resulting field lines around the transmitted current sheet in the 3-D perspective and contours of V_z in the noon meridian plane are plotted in Figures 6a and 6b for t = 70 and 85, respectively. Some closed magnetospheric field lines are also shown. Similar to run 1, the TD is subject to two steps of compression in its interaction with the bow shock and magnetosheath. The second step compression appears to be more profound in the cases with a wider TD.

[31] Just before t = 60, the earthward side of the current sheet has already reached the magnetopause and experienced the second-step compression, while the sunward part of the sheet is still passing through the bow shock. A single X line is later generated right at the nose of the magnetopause. The presence of single X-line reconnection in cases with a wide TD is consistent with the finding by *Omidi et al.* [2009] based on a 2-D global hybrid simulation. The X line at t = 70 can be seen in Figure 6a. The width of the current sheet at the subsolar region has been narrowed down to nearly the same value as that in run 1 after reconnection began. At t = 85, the magnetopause reconnection has been initiated. Note that the magenta field lines in Figure 6b are half open and half closed, in which one end of the field lines is connected to the Earth and the other end connected to the IMF, indicating that the magnetopause has begun to protrude through the region of magnetosheath reconnection. Since the Alfvén speed is larger at the magnetopause than in the magnetosheath, enhanced outflows produced by the magnetopause and magnetosheath reconnection create bulges of field lines and flux ropes. The field lines at the center of the bulges or flux ropes are open field lines with both ends being open to the IMF, as shown by the yellow field lines in Figure 6b, which are surrounded by the magenta ones. Meanwhile, some reconnection has been initiated off the equator plane, as shown by the red field lines in Figure 6b. These structures, however, are convected tailward before they are fully developed.

3.2. Cases With South-to-North Field Direction Change Across TD

[32] We now show cases in which the IMF changes direction from the south to north across the interplanetary TD. In such cases, as the TD passes the bow shock, the region with southward IMF is sandwiched between two regions with a northward magnetic field, the closed geomagnetic dipole field, and the open IMF on the sunward side of TD. As a result, there are two possible ways to consume the southward component of magnetic fluxes through magnetic reconnection: Reconnection processes at the magnetopause and in the magnetosheath.

[33] Figure 7 shows field lines at the magnetopause and in the magnetosheath obtained at t = 60 and 75 from run 3, which is similar to run 1, with $w = 1\ R_E$, except for a south-to-north field change with $\Delta\Phi = -180°$ across the interplanetary TD. Also shown in Figure 7 are the corresponding ion density contours in the noon meridian plane at both times and some density isosurfaces for t = 75. The subsolar part of TD passes through the bow shock completely by t = 40, with its central width being narrowed down to 0.8 R_E, similar to run 1. The magnetosheath reconnection is initiated at t = 45, while magnetopause reconnection begins at t = 20. The occurrence of reconnection at the magnetopause and in the magnetosheath can be seen from the flux ropes in Figure 7a for t = 60. The red field lines are the ones connecting to the Earth, while the yellow ones are the

ones with both ends open to the IMF. The scale sizes of the magnetopause flux rope are comparable to those of the magnetosheath flux ropes. The field lines in the transmitted current sheet stack against the magnetopause.

[34] Later, at $t = 70$, the magnetosheath flux ropes appear to re-reconnect with geomagnetic field lines inside the magnetopause. The re-reconnection has created highly distorted closed field lines, as evidenced by the yellow lines in Figure 7b. As a consequence, high-density, low-temperature magnetosheath ions are captured on these newly formed closed field lines, as indicated by the red isosurfaces of ion density.

[35] Finally, we have also simulated run 4, which is similar to run 3 but for a much larger width of initial TD, $w = 3R_E$. It is found that for such a wide TD, magnetic reconnection at the magnetopause effectively consumes the southward component of the magnetic field. The removal of magnetic flux on the earthward side of TD is faster than the convection of the TD across the bow shock, and no obvious magnetic reconnection signature is obtained in the magnetosheath.

4. Discussions and Conclusions

[36] Directional discontinuity, TD or RD, is a frequently recurring phenomenon in the solar wind. The magnetosheath reconnection provides an alternative way for TD to interact with the magnetopause. In our simulation, the north–south component of IMF fluxes can propagate around the magnetopause not only along the dawn-dusk direction via magnetosheath convection and/or the magnetopause reconnection, but also along the north–south direction via the magnetosheath reconnection.

[37] Our simulations have shown that patchy reconnection may take place when a relatively thin initial TD passes through the bow shock. An important question is: To what extent do the simulation results represent what could happen in the real Sun-Earth plasma system? Since no reconnection signatures have been found before the TD reaches the bow shock, the compression processes, both the first and the second steps, appear to be some direct reason to initiate the magnetosheath reconnection.

[38] Consider the first step compression or shock compression. The corresponding compression of TD, or compression of the tangentially aligned magnetic flux tubes in the TD, is roughly proportional to the ratio of magnetic field strength across the bow shock. This can be seen from the jump condition of the tangential electric field across the shock. At the subsolar bow shock, in which the normal component of the magnetic field $B_n \approx 0$, such a jump condition

$$\left[u_n \vec{B}_t\right] = 0 \tag{3}$$

states the conservation of tangential magnetic field flux, which leads to

$$B_{t2}/B_{t1} = v_{n2}/v_{n1} = n_2/n_1 = \gamma, \tag{4}$$

where v is the bulk velocity, γ is the compression ratio of the shock, and subscripts t, n, 1, and 2 represent the tangential-component, normal-component, upstream, and downstream quantities, respectively. Correspondingly, the flux tube should be narrowed nearly by the factor of γ across the bow shock.

[39] On the other hand, inside the transmitted TD, the diverging magnetosheath flows convect the plasma and magnetic flux away from the subsolar region, poleward and tailward along the TD plane. In our cases, the magnetic field possesses a circular polarization through the TD, and the magnetic flux at the center of the current sheet is dominated by B_y. Once this localized B_y is removed, the reduction of magnetic pressure results in further narrowing of the current sheet because of the total pressure balance. In the cases in which the plasma thermal pressure dominates the TD transition layer, the removal of plasma due to the divergent flow would also result in a similar reduction of total pressure and thus the TD width.

[40] In order to distinguish these two types of compression process, hereinafter we will call the second-step compression the "convective compression." In runs 1 and 3, the magnetic field strength on both sides of the TD increases about 3 times downstream of the bow shock, so the width of the TD has to decrease to about one third of the value in the upstream solar wind, which is $\sim 3.3 d_{i0}$ or $3–4\rho_i$, where ρ_i is the ion Larmor radius in the magnetosheath. Correspondingly, the current density increases 9–10 times on average in the current sheet. Note that reconnection in our hybrid simulation is initiated by a current-dependent resistivity. With some help from the convective compression, the current sheet further contracts, and reconnection is triggered in the sheet soon after it is compressed by the shock. In run 2, on the other hand, the TD is so wide that before its sunward side is transmitted into the magnetosheath, the earthward side of the TD has already reached the magnetopause. The shock compression itself is not enough to drive the magnetosheath reconnection, but a thin current sheet can still be formed because of a dominant role of the convective compression due to the divergent flows in the magnetosheath, and thus the reconnection is initiated.

[41] The Cluster observation by *Phan et al.* [2007] has shown that even for a rather wide TD or current sheet (about 3 R_E or $260 d_{i0}$) in the interplanetary space, it could be significantly narrowed so as to trigger a merging process while the TD traverses the bow shock and impacts the magnetopause. The compression due to the bow shock and the magnetopause, by a factor of 5, would imply a half-width of the compressed current sheet of about 1300–1800 km. For a typical magnetosheath with $B = 30$ nT, $T_i = 1$ keV, and thus the ion gyroradius $\rho_i \approx 153$ km, the current sheet appears to be too wide to allow the occurrence of reconnection. In fact, the observation shows that the width of the current sheet in the magnetosheath reconnection at the Cluster crossing is reduced by a factor of 36, which seems to be consistent with our suggestion that the convective compression may not only have played an important role in the thinning of the TD, but it could indeed also be the dominant thinning mechanism.

[42] The scale length d_i used in our simulation, although <1% of the curvature radius of the dayside magnetosphere, is about 6 times that in reality. The half-width of the initial TD in run 1 is $10 d_{i0}$, whereas in the observed case the half-width of the solar wind TD is about $88 d_{i0}$. The solar wind convection speed in the simulation is 6 times faster than the

typical value in reality due to the larger Alfvén speed used in the simulation. The larger convection speed leads to a shorter convection time in the magnetosheath, whose global size is of a realistic scale length. As a result, the prescribed smaller width of TD seems to be offset by its shorter interaction time with the bow shock and the magnetosheath. We have also run case 1 with d_{i0} and grid sizes being reduced by 50%, and the results appear to be qualitatively the same, with the spatial lengths of physical structures scaled to the smaller d_{i0} and ρ_i. Nevertheless, the larger convection speed also means a faster magnetic flux removal in the transmitted current sheet due to the reconnection flow. Thus, due to the scaling effects, the occurrence of magnetosheath reconnection in the simulation may be earlier than that in reality after the solar wind TD interacts with the bow shock. Another factor that may contribute to the tearing instability associated with magnetic reconnection is the strong temperature anisotropy downstream of the quasi-perpendicular bow shock, which can be seen in Figures 4b and 4c. It has been suggested that the temperature anisotropy can strongly increase the linear growth rate of tearing mode instability [*Shi et al.*, 1987; *Ambrosiano*, 1986].

[43] In the satellite observation of *Phan et al.* [2007], only Cluster 1 observed a clear evidence of magnetosheath reconnection, while the other three satellites, 1–2 R_E away from it, did not detect any signature of the merging process, indicating that the reconnection is quite localized. Meanwhile, the current sheet width observed by Cluster 4 was 2–3 times wider than that observed by Cluster 1. A greater decrease in the magnetic field strength at the center of the thinner current sheet was found by Cluster 1, 2, and 3, while a moderate decrease was found by Cluster 4 in the wider current sheet. This measurement may be consistent with our result in that the reconnection flow will carry the Y-component flux more efficiently than any other region and may cause additional thinning near the X line.

[44] The question of how thin a TD can be before the magnetosheath reconnection is triggered is beyond the capability of our simulation. In addition to the scaling effects mentioned above, the electron kinetic physics is not included in the hybrid model. The smallest resolvable width of the local sheet cannot be below several grid sizes of 0.09 R_E. Note that the hybrid model is valid for the kinetic physics of $k\rho_i \sim 1$.

[45] An interesting feature is obtained for the cases with a south-to-north field change across TD. In such cases, magnetopause reconnection effectively consumes the southward component of magnetic fluxes in the magnetosheath, and the magnetopause is much easier to be penetrated by the magnetosheath current sheet. In runs 3 and 4, the southward magnetic flux on the earthward side of the magnetosheath current sheet has been consumed completely by $t = 70$, when the sheet begins to interact with the magnetopause. Clearly, at the magnetopause, the Alfvén speed is larger than that in the magnetosheath, which leads to a larger reconnection rate or the ability of consuming the southward magnetic flux. Reconnection processes at the magnetopause and in the magnetosheath compete with each other. For a rather wide TD, as in run 4, no clear reconnection signature has been found in the magnetosheath.

[46] On the other hand, for the cases with a north-to-south field change, magnetosheath reconnection can be initiated even for a rather wide TD. This result indicates that in such cases the time duration for the last open flux tube on the earthward side of the TD to leave the dayside, after the solar wind TD reaches the bow shock, is longer than the time for reconnection to occur in the magnetosheath. Compared to the south-to-north case, in the north-to-south case the time for the open fluxes on the earthward side of the current sheet to stay in the dayside magnetosheath is nearly their entire convection time from the bow shock to the magnetopause. Moreover, it is well known that under a northward IMF, a density depletion layer is present in front of the magnetopause because of the pileup of field lines. According to *Zwan and Wolf* [1976], in the plasma depletion layer, "the nearer a flux tube trajectory comes to the stagnation point, the longer the tube resides in the magnetosheath and the closer it comes to the magnetopause." Such an effect would also allow the TD to stay longer in the dayside magnetosheath and thus lead to a more frequent occurrence of magnetosheath reconnection in north-to-south cases than in the south-to-north cases. For all the cases in our simulation, the solar wind TD starts to pass the bow shock around $t = 35$. In run 1, the last open flux tube on the earthward side of the magnetosheath merging layer disappears from the dayside around $t = 80$–85, which also marks the beginning of the magnetopause reconnection, while in run 3 the magnetosheath flux ropes start to interact with the magnetopause at an earlier $t = 75$.

[47] Complicated flux ropes may be produced via patchy reconnection in the magnetosheath. The motion of these flux ropes is determined by the reconnection flow and magnetosheath flow, largely along the plane of current sheet in the rest reference frame of the discontinuity. Consider a satellite that is located in the subsolar magnetosheath but still relatively far from the magnetopause. The passage of magnetosheath flux ropes is likely along the direction normal to the current sheet due to the convection in the $-X$ direction, which means that no bipolar B_N signature of FTEs would likely be detected. When these flux ropes further propagate near the magnetopause, however, their convection is predominantly along the magnetopause, similar to the motion of a magnetopause flux rope, while the normal direction of the current sheet in the local LMN coordinates is roughly normal to the magnetopause. In this situation, the flux orientation relative to its motion may provide an opportunity for spacecraft near the magnetopause to observe the bipolar-B_N structure of magnetosheath FTEs. Furthermore, unlike the magnetopause flux ropes, no mixture of the magnetospheric and magnetosheath plasmas would be observed in ion phase-space spectra in a magnetosheath flux rope, even on the earthward side of the flux ropes. Instead, enhancement of plasma density accompanied by a moderate enhancement of ion temperature could be viewed as characteristics of the magnetosheath flux ropes.

[48] For a TD with a south-to-north field change, spacecraft in the magnetosheath may observe opposite bipolar field senses, more complicated than the structures in the usual magnetosheath FTEs of magnetopause flux ropes. The curvature vector of magnetic field lines in flux ropes may be measured by Cluster spacecraft, provided that the distances among the satellites are small enough. In particular, for Cluster spacecraft located on the earthward side of the transmitted solar wind, the curvature vector [*Shen et al.*, 2003] of

magnetosheath field lines could be observed to point sunward instead of earthward. Such a feature can also be utilized to identify flux ropes in the magnetosheath reconnection.

[49] In summary, we have presented global hybrid simulation results of the interaction between a circularly polarized interplanetary tangential discontinuity and the bow shock/magnetopause. Cases with a northward or southward initial IMF are discussed, and the magnetic field orientation is assumed to change by 180° across the interplanetary directional TD. The following conclusions are obtained.

[50] 1. While the TD is transmitted through the bow shock into the magnetosheath, it is narrowed by a two-step compression process, the shock compression and the convective compression. The degree of compression by the former one is proportional to the compression ratio of the bow shock, while the latter may play a dominant role in the thinning of the current sheet. Magnetosheath reconnection occurs in the narrowed, thin current sheet.

[51] 2. The magnetosheath reconnection is of a patchy type for cases with a relatively thin TD in the solar wind. In cases with either a north-to-south or a south-to-north field direction change across the TD, the patchy reconnections are initiated before the TD reaches the magnetopause. In the cases with a south-to-north field change, both the magnetopause reconnection and magnetosheath reconnection may take place simultaneously. The two reconnection processes will compete with each other to consume the southward magnetic field.

[52] 3. For cases with a relatively wide initial TD, the north-to-south and south-to-north field rotations lead to drastically different results. In the north-to-south case, a dominant X line appears at the nose in front of the magnetopause and some weaker reconnection X lines off the equator are convected tailward before they are fully developed. In the south-to-north case, however, reconnection may cease to exist in the transmitted TD in the magnetosheath because the removal of the southward component of the magnetosheath field by the magnetopause reconnection is faster than the contraction of the transmitted TD.

[53] 4. The scale lengths of the magnetosheath flux ropes are comparable to those of the magnetopause flux ropes in both the latitudinal and radial directions, but larger than the sizes of magnetopause ropes in the dawn-dusk direction. In particular, in the south-to-north case, the reconnected magnetosheath field lines can re-reconnect with the geomagnetic field lines at the magnetopause, creating newly reformed closed field lines. Such a process leads to the capture of magnetosheath plasma in the magnetosphere, which provides an additional mechanism to transfer the solar wind mass and momentum into the magnetosphere and contributes to the formation of the magnetopause boundary layer.

[54] **Acknowledgments.** This work was supported by NSF grant ATM-0646442 to Auburn University and National Natural Science Foundation of China (NSFC) grant 40640420563 to Wuhan University. Computer resources were provided by the Arctic Region Supercomputer Center.

[55] Zuyin Pu thanks the reviewer for their assistance in evaluating this paper.

References

Ambrosiano, J. (1986), Simulation of the collisionless tearing instability in an anisotropic neutral sheet, *J. Geophys. Res.*, *91*, 113–120, doi:10.1029/JA091iA01p00113.

Borg, A. L., M. Øieroset, T. D. Phan, F. S. Mozer, A. Pedersen, C. Mouikis, J. P. McFadden, C. Twitty, A. Balogh, and H. Rème (2005), Cluster encounter of a magnetic reconnection diffusion region in the near-Earth magnetotail on September 19, 2003, *Geophys. Res. Lett.*, *32*, L19105, doi:10.1029/2005GL023794.

Burlaga, L. F., J. F. Lemaire, and J. M. Turner (1977), Interplanetary current sheets at 1 AU, *J. Geophys. Res.*, *82*, 3191–3200, doi:10.1029/JA082i022p03191.

Dungey, J. W. (1961), Interplanetary magnetic field and the auroral zones, *Phys. Rev. Lett.*, *6*, 47–48, doi:10.1103/PhysRevLett.6.47.

Fu, X. R., Q. M. Lu, and S. Wang (2006), The process of electron acceleration during collisionless magnetic reconnection, *Phys. Plasmas*, *13*, 012309, doi:10.1063/1.2164808.

Gosling, J. T., R. M. Skoug, D. J. McComas, and C. W. Smith (2005), Direct evidence for magnetic reconnection in the solar wind near 1 AU, *J. Geophys. Res.*, *110*, A01107, doi:10.1029/2004JA010809.

Hoshino, M., T. Mukai, Y. Yamamoto, and S. Kokubun (1998), Ion dynamics in magnetic reconnection, Comparison between numerical simulation and Geotail observations, *J. Geophys. Res.*, *102*(A3), 4509–4530.

Krauss-Varban, D., and N. Omidi (1995), Large-scale hybrid simulations of the magnetotail during reconnection, *Geophys. Res. Lett.*, *22*, 3271–3274, doi:10.1029/95GL03414.

Lee, L. C. (1995), A review of magnetic reconnection, in *Physics of the Magnetosphere*, *Geophys. Monogr. Ser.*, vol. 90, edited by B. U. Ö. Sonnerup and M. F. Thomsen, p. 139, AGU, Washington, D. C.

Lin, Y. (1997), Generation of anomalous flows near the bow shock by the interaction of interplanetary discontinuities, *J. Geophys. Res.*, *102*, 24,265–24,281, doi:10.1029/97JA01989.

Lin, Y. (2001), Global hybrid simulation of the magnetopause reconnection layer and associated field-aligned currents, *J. Geophys. Res.*, *106*, 25,451–25,465, doi:10.1029/2000JA000184.

Lin, Y., and D. W. Swift (1996), A two-dimensional hybrid simulation of the magnetotail reconnection layer, *J. Geophys. Res.*, *101*, 19,859–19,870, doi:10.1029/96JA01457.

Lin, Y., and X. Y. Wang (2005), Three-dimensional global hybrid simulation of dayside dynamics associated with the quasi-parallel bow shock, *J. Geophys. Res.*, *110*, A12216, doi:10.1029/2005JA011243.

Lin, Y., and X. Y. Wang (2006), Formation of dayside low-latitude boundary layer under northward interplanetary magnetic field, *Geophys. Res. Lett.*, *33*, L21104, doi:10.1029/2006GL027736.

Linton, M. G., and D. W. Longcope (2006), A model for patchy reconnection in three dimensions, *Astrophys. J.*, *642*, 1177–1192, doi:10.1086/500965.

Lottermoser, R. F., M. Scholer, and A. P. Matthews (1998), Ion kinetic effects in magnetic reconnection: Hybrid simulations, *J. Geophys. Res.*, *103*, 4547–4559, doi:10.1029/97JA01872.

Lyons, L. R., G. T. Blanchard, J. C. Samson, R. P. Lepping, T. Yamamoto, and T. Moretto (1997), Coordinated observations demonstrating external substorm triggering, *J. Geophys. Res.*, *102*, 27,039–27,051, doi:10.1029/97JA02639.

Maynard, N. C., et al. (2002), Predictions of magnetosheath merging between IMF field lines of opposite polarity, *J. Geophys. Res.*, *107*(A12), 1456, doi:10.1029/2002JA009289.

Øieroset, M., H. Lühr, J. Moen, T. Moretto, and P. E. Sandholt (1996), Dynamical auroral morphology in relation to ionospheric plasma convection and geomagnetic activity: Signatures of magnetopause X line dynamics and flux transfer events, *J. Geophys. Res.*, *101*, 13,275–13,292, doi:10.1029/96JA00613.

Øieroset, M., T.-D. Phan, M. Fujimoto, and R. P. Lepping (2001), In situ detection of collisionless reconnection in the Earth's magnetotail, *Nature*, *412*, 414–417, doi:10.1038/35086520.

Omidi, N., and D. G. Sibeck (2007), Flux transfer events in the cusp, *Geophys. Res. Lett.*, *34*, L04106, doi:10.1029/2006GL028698.

Omidi, N., T. Phan, and D. G. Sibeck (2009), Hybrid simulations of magnetic reconnection initiated in the magnetosheath, *J. Geophys. Res.*, *114*, A02222, doi:10.1029/2008JA013647.

Otto, A. (1995), Forced three-dimensional magnetic reconnection due to linkage of magnetic flux tubes, *J. Geophys. Res.*, *100*, 11,863–11,874, doi:10.1029/94JA03341.

Phan, T.-D., et al. (2006), A magnetic reconnection X-line extending more than 390 Earth radii in the solar wind, *Nature*, *439*, 175–178, doi:10.1038/nature04393.

Phan, T. D., G. Paschmann, C. Twitty, F. S. Mozer, J. T. Gosling, J. P. Eastwood, M. Øieroset, H. Rème, and E. A. Lucek (2007), Evidence for magnetic reconnection initiated in the magnetosheath, *Geophys. Res. Lett.*, *34*, L14104, doi:10.1029/2007GL030343.

Pritchett, P. L. (2006), Relativistic electron production during guide field magnetic reconnection, *J. Geophys. Res.*, *111*, A10212, doi:10.1029/2006JA011793.

Retin, A., D. Sundkvist, A. Vaivads, F. Mozer, M. André, and C. J. Owen (2007), In situ evidence of magnetic reconnection in turbulent plasma, *Nat. Phys.*, *3*, 235–238.

Russell, C. T., and R. C. Elphic (1979), ISEE observations of flux transfer events at the dayside magnetopause, *Geophys. Res. Lett.*, *6*(1), 33–36.

Shen, C., X. Li, M. Dunlop, Z. X. Liu, A. Balogh, D. N. Baker, M. Hapgood, and X. Wang (2003), Analyses on the geometrical structure of magnetic field in the current sheet based on cluster measurements, *J. Geophys. Res.*, *108*(A5), 1168, doi:10.1029/2002JA009612.

Shi, Y., L. C. Lee, and Z. F. Fu (1987), A study of tearing instability in the presence of a pressure anisotropy, *J. Geophys. Res.*, *92*, 12,171–12,179, doi:10.1029/JA092iA11p12171.

Sonnerup, B. U. Ö., and L. J. Cahill (1967), Magnetopause structure and attitude from Explorer 12 observations, *J. Geophys. Res.*, *72*(1), 171–183.

Sonnerup, B. U. Ö., G. Paschmann, and T.-D. Phan (1995), Fluid aspects of reconnection at the magnetopause: In situ observations, in *Physics of the Magnetopause*, *Geophys. Monogr. Ser*, vol. 90, 167 pp., AGU, Washington, D. C.

Swift, D. W. (1996), Use of a hybrid code for a global-scale plasma simulation, *J. Comput. Phys.*, *126*, 109–121, doi:10.1006/jcph.1996.0124.

Thomsen, M. F., J. E. Borovsky, and R. M. Skoug (2003), Delivery of cold, dense plasma sheet material into the near-Earth region, *J. Geophys. Res.*, *108*(A4), 1151, doi:10.1029/2002JA009544.

Zwan, B. J., and R. A. Wolf (1976), Depletion of solar wind plasma near a planetary boundary, *J. Geophys. Res.*, *81*, 1636–1648, doi:10.1029/JA081i010p01636.

X. H. Deng and Y. Pang, Department of Space Physics, Wuhan University, Wuhan 430072, China.

Y. Lin, B. Tan, and X. Y. Wang, Physics Department, Auburn University, 206 Allison Laboratory, Auburn, AL 36830-5429, USA. (ylin@physics.auburn.edu)